New Aspects of Technical Testing of Intravascular Stents

V. I. Sergienko, A. K. Martynov, A. V. Petryaikin, D. S. Koshurnikov, A. A. Fadeev*, D. A. Nikolaev*, G. G. Karmazanovskii, N. Yu. Osipova**, and V. D. Fedorov****

Translated from *Byulleten' Eksperimental'noi Biologii i Meditsiny*, Supplement 2, pp. 112-116, April, 2007
Original article submitted February 18, 2006

Maximum magnetic resonance artifacts from stents are often determined by the presence of ferromagnetic compounds in the delivery system. We propose a mathematic model describing artifacts caused by nitinol stents. A method for evaluation of critical radial rigidity of the stents was developed.

Key Words: *stent; magnetic resonance imaging; artifacts; Nitinol; radial rigidity*

Intravascular stent is an implanted netted cylindrical structure maintaining the patency of a blood vessel. Special stents are designed for maintaining biliary tracts (biliary stents), urinary tracts (uretral stents), *etc.* There are no universal standard methods for preclinical evaluation and technical testing of intravascular stents. This can be explained by great variety of their constructions and great number of parameters for their evaluation. These parameters include biocompatibility and hemocompatibility of the stent material (evaluation of biological effects of materials according to GOST RICO 10993-99), mechanical properties of construction, geometrical characteristics, X-ray contrast properties and magnetic resonance (MR) compatibility of the stent, as well as requirements to the stent delivery system [10].

The development of methods of clinical testing is a fundamental problem, because it will help to propose a substantiated system for evaluation of the safety of clinical use of not only intravascular stents, but also other implanted wire constructions and to avoid complication. The development of new systems and methods of MR-guided stent delivery without traditional X-ray control will help to avoid irradiation of the patient and staff and to reduce the doses of contrast agents or completely abolish it. These studies are in progress in some research centers [3,5,11,12]. Modeling of the behavior of MR signal near the stent and analysis of critical mechanical parameters are necessary for further progress in this field.

Studies of MR imaging and mechanical properties of stents were performed at the Laboratory of Experimental Hemosorption and Oxidative Methods of Detoxification, Institute of Physicochemical Medicine in collaboration with A. V. Vishnevskii Institute of Surgery and A. N. Bakulev Research Center of Cardiovascular Surgery.

MATERIALS AND METHODS

MR imaging was performed on a Giroscan Intera 1,0 T. tomograph (Philips). For visualization of the stent in a flow we used a non-magnetic phantom allowing regulation of the flow rate in a wide range (0-1 liter/min). The construction of the phantom ensured system reliability and precision of the results. Degassed and deionized water was used as the liquid medium.

A vascular endoprotesis Hemobahn (W.L.Gore& Associes, S.A.R.L.) made of stretched polytetrafluoroethylene coated with Nitinol framework along its external surface (10 cm endoprosthesis length, 8 mm internal diameter) was studied. MR scanning

Laboratory of Experimental Hemosorption and Oxidative Methods of Detoxification, Research Institute of Physicochemical Medicine, Federal Agency for Health Care and Social Development; *Laboratory on the Use of Polymers in Cardiovascular Surgery, A. N. Bakulev Research Center of Cardiovascular Surgery, Russian Academy of Medical Sciences; **Department of Radiation Diagnostics, A. V. Vishnevskii Institute of Surgery, Moscow

0007-4888/07/1443-0482

of the water-filled phantom with positioned endoprosthesis in a gradient-echo mode (7.1 msec repetition time, 3.5 msec echo) and phase-contrast MR angiography (MRA, 81 msec repetition time, 9 msec echo) were performed.

We also tested a coarse-meshed braided stent (Komed) in the MRA regimen. The length and diameter of the stent in the expanded state are 22.4 and 4.9 mm, respectively. Standard T1- and T2-weighted MR imaging and 3D phase contrast MRA were performed (20 msec repetition time, 8 msec echo). MR signal was measured relatively to immobile water, the calculated magnitude of the signal (S_{rel}) was plotted as a profile measured in the center of the water-filled tube along the stent.

For evaluation of mechanical strength of the construction, radial rigidity of Penta Multilink (Guidant) and Nexus (Occam) stents was measured. This test determines the limit of elasticity of the stent during its radial deformation. The stents were expanded in a regimen recommended by the manufacturer and the placement system was removed. Before testing, the length of the sample was measured with a caliper. The compression test was performed on a Zwick/Roell tearing machine. The sample was placed between the pushing plates and gradually compressed at a rate of 0.2 mm/sec; the sample deformation was continuously recorded. Diagrams illustrating the relationships between compression forces and diameter deformation were constructed, an initial linear fragments corresponding to stent elasticity and subsequent linear fragment corresponding to plastic deformation were isolated. The ratio of elasticity limit to the length of the stent was determined.

RESULTS

Problems of visualization of intravascular stents of various constructions during MRI and MRA are now actively discussed. This is related to safety and diagnostic efficiency of MRI in patients with stents [1,4,6,8]. A number of reports describe MR-guided stent placement in arteries of different diameters under experimental and clinical conditions and installation of nonvascular stents. Impressive results in this field were obtained [2,3,5,9,11,12].

The most important negative effects of stents during MRI are heating during interaction with radio-frequency and gradient fields, displacement and mechanical rotation of the stent in constant magnetic field and its gradient, and various artifacts distorting images of the stented vessel and adjacent regions.

There are no methods of quantitative evaluation of these artifacts probably because of complex construction of the stents.

We showed that artifacts determined by components of the delivery system are highly pronounced and cannot be quantitatively described (Fig. 1,

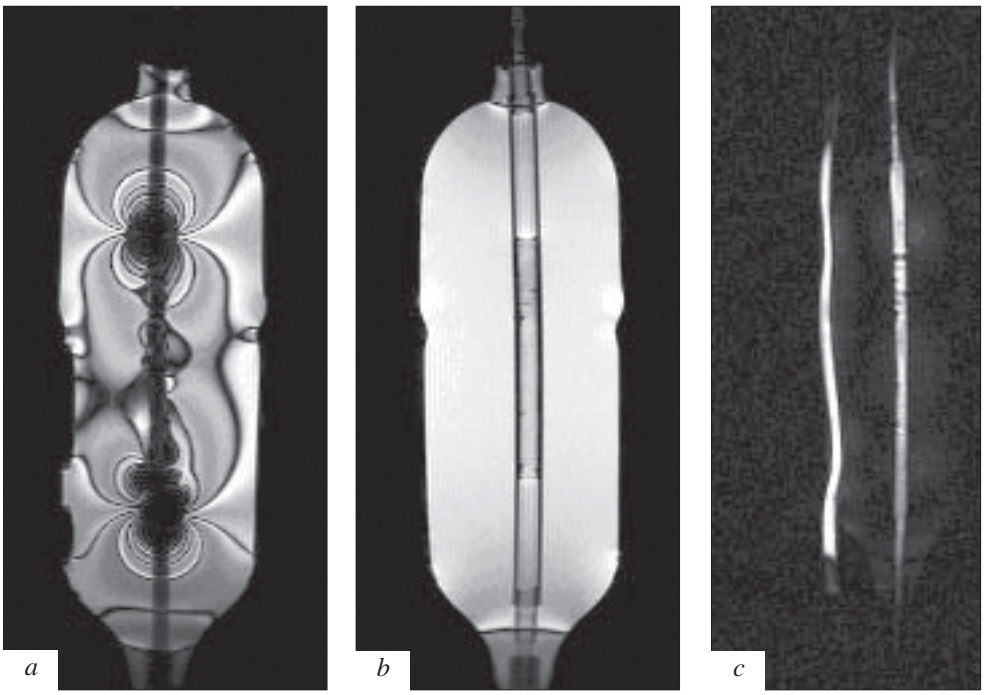

Fig. 1. MR imaging of water-filled phantom with a stent. *a, b*) gradient echo scanning, repetition time 7.1 msec, echo 3.5 msec. *a*) artifacts from the stent delivery system; *b*) the same stent in expanded state without delivery system, no pronounced artifacts are seen; *c*) phase-contrast MRA, repetition time 81 msec, echo 9 msec, volume flow rate 1 liter min, stent with artifacts from Nitinol braiding is seen.

a). The studied system contains ferromagnetic markers of the stent position. The artifacts were less pronounced without stent delivery system (Fig. 1, *b*), but they cannot be described in an analytic form due to complex braiding of the Nitinol framework.

At the next stage we studied artifacts of MPA images of vascular stents, which were typically presented by alternating dark and light bands along the tube with the stent. Minimums of MP signal, dark bands, corresponded to areas of Nitinol thread twisting (Fig. 1, *c*; 2, *a*), which agrees with published data [6,7] indicating reduced signal in sites corresponding to wire fragments perpendicular to the major field of magnet B_0.

Coarse-meshed braided Nitinol stent was used as the model object. The arrangement of its threads is described by a cosine function (Fig. 2, *a*, *b*). The longitudinal axis of the stent in the experiment was oriented along the field.

The position of artifacts can be calculated from the pattern of stent braiding as follows. If the Nitinol thread follows a cosine curve: $x(y)=\cos(y)$, the fragment marked on Fig. 2, *b* and presented on Fig. 2, *c* in blowup and 90° turned view is described by an equation: $y(x)=\arccos(x)$.

In points of twisting the wire is positioned in such a way, that its projection on ordinate axis is maximum: as seen from the figure $\Delta y_1>\Delta y_2$. This explains decreased signal in twisting points. During the experiment the tube with the Nitinol stent was arranged along B_o field, along the ordinate axis. As follows for previous reports [6,7], the artifacts reducing the signal are maximum when the Nitinol wire is perpendicular to B_o field. The zones of reduced signal correspond to Nitinol thread twisting points on the stent image (Fig. 2, *a*).

The projection of a small mesh section of the ordinate axis is equal to the product of Δx and $\arccos(x)$ derivative (Fig. 2, *c*).

$$\Delta y=\Delta x\times(\sqrt{\arccos(x)}),$$

or

$$\Delta y=\Delta x\times 1/(\sqrt{(1-x^2)}).$$

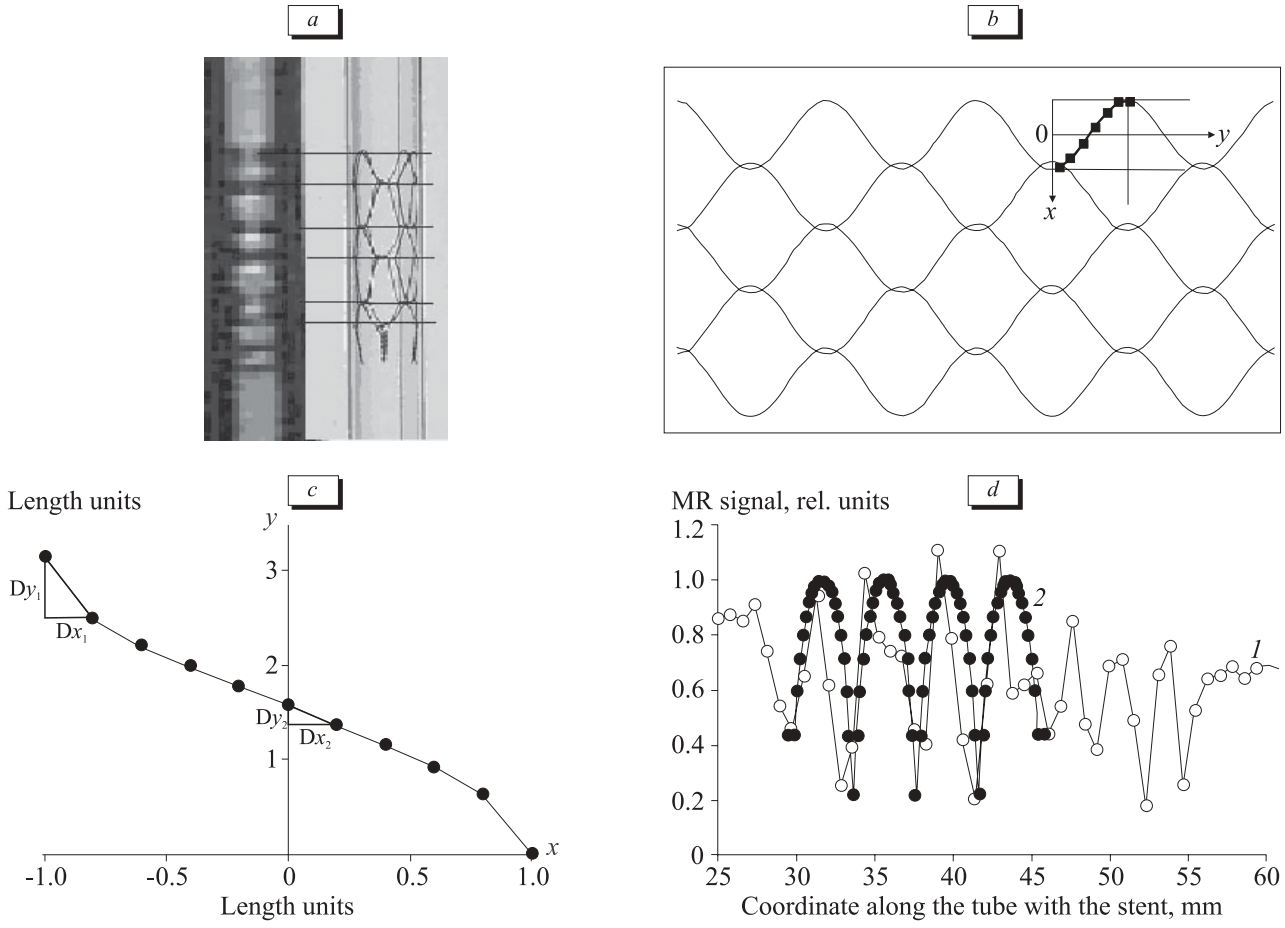

Fig. 2. Effect of braiding structure of the Nitinol stent on MR artifacts.*a*) 3D phase-contrast MRA, repetition time 20 msec, echo 8 msec; MRA is compared with a photo of the stent in the same scale; *b*) scheme of braiding of Nitinol threads ; *c*) fragment of braiding of coarse-meshed Nitinol stent; *d*) comparison of relative MR signal along the tube with the stent (*1*) and calculated intensity of the signal (*2*).

Then the relative signal (S_{rel}) is proportional to a value reciprocal to Δy:

$$S_{rel}=k\times(\sqrt{(1-x^2)}), \quad (1)$$

$k=n\times m$, where n is the number of analyzed half-periods of braiding (n=8 in our case) and m is a normalization factor. The k factor standardizes the obtained relationship for S_{rel} from the tube with the stent. Modeling was performed within regular structure of the stent and did not include 45-55-mm terminal fragments.

In flexion points of the Nitinol thread x=1 or x=-1, $S_{rel}(x)\rightarrow 0$. However, this was not the case. In further calculations the signal in these points was taken equal to the previous y value. We also assumed that in twisting points the wire material doubles.

S_{rel} calculated from equation (1) agrees with the results of direct measurements of the signal along the tube profile (Fig. 2, *d*).

Finally, we studied mechanical properties of vascular stents. The vascular stent (according to definition) is designed for maintaining the vessel lumen in an open state under conditions of mechanical load and various defects of the vascular wall (calcification, atherosclerotic plaques, stenoses). We studied deformations of the stent during external mechanical compression, which in living organism can be caused by tumor growth around the stented vessel. For evaluation of mechanical properties we chose the test for measuring elasticity limit. For measuring minimal permissible level of elasticity (F_{MIN}) we used the following equation:

$$(F_{MIN})/L=P_{MAX}\times D, \quad (2)$$

where P_{MAX} is the maximum pressure in the stented vessel (~20 kPa) and D is stent diameter. For a stent with a diameter of 3 mm, F/L should be $\geq$0.06 N/mm. The limit of elasticity can be determined as a compression force corresponding to the flexion point of the curve (Fig. 3). For Penta Multilink and Nexus these values were 5 and 1.32 N, respectively. After standardization per unit of stent length, the values of the relative elasticity limit were 0.28 and 0.11 N/mm, respectively. These values exceeded the critical value 0.06 N/mm calculated for critical physiological conditions according to equation (2). The tested stents met the requirements with a considerable load factor.

Thus, maximum artifacts from the stents are often determined by the presence of ferromagnetic substances in the stent delivery systems, which should be taken into account during MR-guided stent placement.

For the tested stents, the critical radial rigidity far surpassed that for vessels of the corresponding diameter and critical physiological pressure conditions.

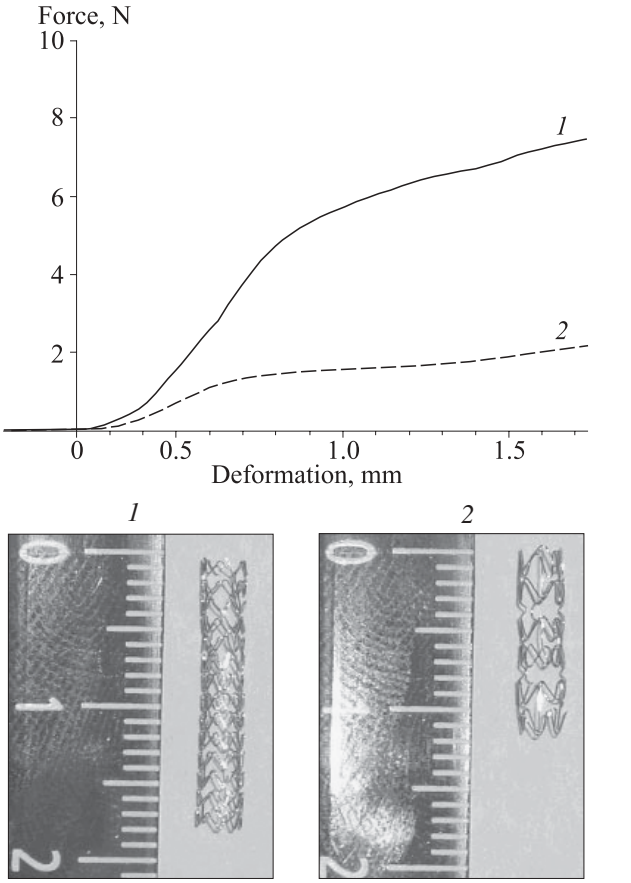

Fig. 3. Radial rigidity of Penta Multilink (*1*) and Nexus (*2*) stents.

REFERENCES

1. L. W. Bartels, H. F. Smits, C. J. Bakker, and M. A. Virgever, *J. Vasc. Interv. Radiol*., **12**, No. 3, 365-371 (2001).
2. H. Eggebrecht, G. Heusch, R. Erbel, *et al., Basic Res. Cardiol.*, **102**, No. 1, 1-8 (2007).
3. D. R. Elgort, C. M. Hillenbrand, S. Zhang, *et al., J. Magn. Reson. Imaging*., **23**, No. 5, 619-627 (2006).
4. S. Hahnel, T. H. Nguyen-Trong, S. Rohde, *et al., J. Neuroradiol*., **33**, No. 2, 75-80 (2006).
5. C. B. Henk, C. B. Higgins, and M. Saeed, *J. Magn. Reson. Imaging*., **22**, No. 4, 451-460 (2005).
6. M. Lenhart, M. Volk, C. Manke, *et al., Radiology*, **217**, No. 1, 173-178 (2000).
7. L. Letourneau-Guillon, G. Soulez, G. Beaudoin, *et al., J. Vasc. Interv. Radiol*., **15**, No. 6, 615-624 (2004).
8. D. Maintz, B. Tombach, K. U. Juergens, *et al., AJR Am. J. Roentgenol*., **179**, No. 5, 1319-1322 (2002).
9. E. R. McVeigh, M. A. Guttman, R. J. Lederman, *et al., Magn. Reson. Med*., **56**, No. 5, 958-964 (2006).
10. *Non-clinical tests and recommended labeling for intravascular stents and associated delivery systems. U.S.* Department of Health and Human Services, Food and Drug Administration, Center for Devices and Radiological Health, 2005.
11. C. Ozturk, M. Guttman, E. R. McVeigh, and R. J. Lederman, *Top Magn. Reson. Imaging*., **16**, No. 5, 369-381 (2005).
12. M. Saeed, C. B. Henk, O. Weber, *et al., J. Magn. Reson. Imaging*., **24**, No. 2, 371-378 (2006).